Journal of Catalysis 381 (2020) 570–578

Contents lists available at ScienceDirect

Journal of Catalysis

journal homepage: www.elsevier.com/locate/jcat

Insights into the active sites and catalytic mechanism of oxidative esterification of 5-hydroxymethylfurfural by metal-organic frameworks-derived N-doped carbon

Yunchao Feng [a], Wenlong Jia [a], Guihua Yan [a], Xianhai Zeng [a,b,c,*], Jonathan Sperry [d], Binbin Xu [e], Yong Sun [a,b,c], Xing Tang [a,b,c], Tingzhou Lei [f], Lu Lin [a,b,c]

[a] College of Energy, Xiamen University, Xiamen 361102, China
[b] Fujian Engineering and Research Center of Clean and High-valued Technologies for Biomass, Xiamen 361102, China
[c] Xiamen Key Laboratory of Clean and High-valued Utilization for Biomass, Xiamen 361102, China
[d] Centre for Green Chemical Science, University of Auckland, Auckland 1142, New Zealand
[e] College of Chemistry and Chemical Engineering, Xiamen University, Xiamen 361102, China
[f] Henan Key Lab of Biomass Energy, Huayuan Road 29, Zhengzhou, Henan 450008, China

ARTICLE INFO

Article history:
Received 26 September 2019
Revised 12 November 2019
Accepted 19 November 2019
Available online 18 December 2019

Keywords:
5-Hydroxymethylfurfural
Dimethyl furan dicarboxylate
Mechanism
Oxidation
Catalysis

ABSTRACT

Directly oxidative esterification of Biomass-derived 5-hydroxymethylfurfural (HMF) into dimethyl furan dicarboxylate (DMFDCA) is a promising route for the replacement of petroleum-derived commodity chemical terephthalic acid (TPA) extensively employed in polyester synthesis. Co-based N-doped carbon materials are one of the most promising applied catalysts for oxidative esterification reaction, however, the active sites and reaction pathway of these catalysts have not been clearly clarified, which is crucial to the practical application. Herein, we report that ZIF-67 (a zeolitic imidazolate framework (ZIF)-type cobalt-containing MOF) derived Co@C-N material is a highly effective catalyst for the selective conversion of HMF into DMFDCA in 95% yield. The high activity of the ZIF-67 derived nanocarbon composites Co@C-N can be attributed to the electron transfer between nitrogen-doped carbon shells and Co nanoparticles. The appropriate graphitic N and pyridinic N doping increases the electronic mobility and active sites. Density functional theory (DFT) simulations indicated that oxygen, HMF and methanol molecules are adsorbed and activated on C-N materials. Furthermore, no 2, 5-diformylfuran (DFF) was captured as an intermediate because the oxidative esterification of aldehyde preferentially occurred than the oxidation of hydroxyl group in HMF. We anticipate that these results can drive progress in the bio-based polymers sector and oxidative esterification reaction.

1. Introduction

Substituting petroleum-derived terephthalic acid (TPA) with biomass-derived furan-2,5-dicarboxylic acid (FDCA) in polyester production is a longstanding goal in the field of renewable polymer chemistry [1]. The novel polyethylene furandicarboxylate (PEF, prepared from FDCA or its esters) is reported to have superior material properties than polyethylene terephthalate (PET, prepared from TPA), including better biodegradability, higher isolation rate of oxygen, CO_2 and water, higher glass transition temperature and lower melting temperature [2]. Moreover, the production of PEF from lignocellulosic biomass has been predicted to lead to a ~50% reduction in the greenhouse gas emissions associated with current PET production process [3]. Despite great advancements for FDCA production, however, another issue to consider is the poor solubility of FDCA in most industrial solvents. Purification by traditional distillation and recrystallization is unfeasible, hindering the large-scale applications of FDCA [4]. A promising alternative is the direct oxidative esterification of HMF into dimethyl furan dicarboxylate (DMFDCA), which is readily soluble in most common solvents and can be easily purified by sublimation at low-temperature [5]. Furthermore, the production of PEF from DMFDCA is easier to proceed than FDCA.

As the conversion of HMF to DMFDCA can be regarded as the tandem oxidation esterification of a heteroaromatic aldehyde and alcohol, a series of intermediates including 2,5-diformylfuran (DFF), 5-hydroxymethyl-2-methyl-furoate (HMMF) and 5-formyl-2-methyl-furoate (FMF), could be formed (Scheme 1). Indeed,

* Corresponding author at: College of Energy, Xiamen University, Xiamen 361102, China.
E-mail address: xianhai.zeng@xmu.edu.cn (X. Zeng).

https://doi.org/10.1016/j.jcat.2019.11.029
0021-9517/

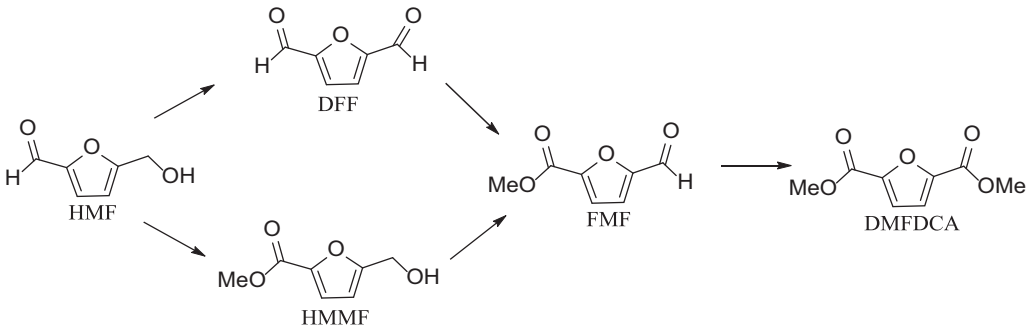

Scheme 1. Reaction pathway for the oxidation esterification of HMF to DMFDCA.

significant research efforts have been reported for the oxidation-esterification of HMF using O_2 and methanol. In 2008, Christensen et al. [4] firstly reported the oxidation esterification of HMF using Au/TiO_2 catalyst, achieving a high DMFDCA yield of 99%. Subsequently, a series of Au or other noble metals based catalysts were employed, providing satisfactory selectivity and yield [6–13]. In 2013, Beller et al. [14] reported that Co_3O_4-N@C was a highly effective catalyst for direct oxidative esterification of alcohols. As a result, unremitting efforts have been devoted to design and synthesis of Co-based N-doped carbon catalysts for the oxidative esterification of alcohols or HMF [15–21]. However, despite these achievements, the active sites and the catalytic pathway of these Co-based catalysts for the oxidative esterification of HMF or alcohols have not been clearly clarified.

Recently, metal-organic frameworks (MOFs), a new class of porous crystalline materials, have emerged as a new platform to synthesize nanocarbon composites for applications as catalysts in electrocatalysis and traditional heterogeneous catalysis [22–25], because of their ordered structures and relatively low thermal stability [26–29]. Based on our recent report on ZIF-8 derived catalysts for hydrogenation of HMF [30], here we report a ZIF-67 derived nanoscale Co-based catalysts (Co@C-N) for the oxidation of HMF to DMFDCA (>99% conversion and 95% yield). ZIF-67 was selected as a catalyst precursor also because of its abundant carbon and nitrogen species with zero oxygen content. The detailed experimental analysis, catalysts characterization and DFT simulations shed light on the active sites and reaction mechanism, which we anticipate will drive progress in the bio-based polymers sector and oxidative esterification reaction.

2. Materials and methods

2.1. Materials

All reagents were supplied by Aladdin Chemical Technology Co. Ltd. (Shanghai, China) and used without further purification.

2.2. Synthesis of catalysts

Synthesis of ZIF-67: In a typical synthesis, 0.65 g of $Co(NO_3)_2 \cdot 6H_2O$ were dissolved in 15 mL of MeOH/EtOH mixture (1:1) to form a clear solution, which was subsequently poured into 15 mL of MeOH/EtOH mixture (1:1) containing 0.74 g of 2-methylimidazole. After the mixture was stirred for 20 h at room temperature, the as-obtained purple precipitates were centrifuged and washed with EtOH for three times, and finally dried under vacuum at 80 °C for 24 h, resulting in the Co-based zeolitic imidazolate frameworks (ZIF-67).

Synthesis of Co@C-N: The preparation procedure was listed as follow: ZIF-67 was placed in a tube furnace and heated to 300 °C for 2 h, and then pyrolyzed at desired temperature (600, 700, 800 and 900 °C) for 6 h with a heating rate of 5 °C/min under argon atmosphere to obtain Co@C-N(x), where "x" represents the pyrolysis temperature.

Synthesis of Co@C (800): The preparation procedure was as follow: $Co(NO_3)_2 \cdot 6H_2O$ (0.58 g) and trimesic acid (0.15 g) were dissolved in 35 mL of DMF solvent and stirred for 2 h. The obtained light-red solution was then transferred to a 50 mL Teflon autoclave and heated to 120 °C for 24 h. The as-obtained pink precipitates were centrifuged and washed with MeOH for three times, and finally dried under vacuum at 80 °C for 24 h, resulting in the Co-MOF (Co-BTC). Then, after complete pyrolysis at 800 °C (5 °C min^{-1}) for 6 h in argon, Co-BTC derived Co@C was obtained.

2.3. Catalyst characterization

Powder X-ray diffraction patterns of the samples were recorded on a Rigaku D/max X-ray diffractometer using Cu Kα radiation (40 kV, 30 mA, λ = 0.1543 nm). Raman spectra were measured on a Renishaw inVia Raman microscope with 633 nm laser excitation. The laser power was 10 mW, and the spot size was 2 m. BET surface areas measurements were performed with N_2 adsorption/desorption isotherms using a TriStar 3000 with the BET and HK methods. Before measurements, the samples were degassed at 100 °C for 12 h. Element contents of the samples were determined using an Elementar Vario EL III instrument and Inductively Coupled Plasma Optic Emission Spectrometer (ICP-OES, Varian (720)). The size and morphology of materials were studied by scanning electron microscopy (SEM, SUPRA 55) and high-resolution transmission electron microscopy (HR-TEM, JEM-2100). Thermogravimetry (TG) analysis of ZIF-67 were recorded on an SDT Q600TGA thermal gravimetric analyzer under N_2. The magnetic properties of Co@C-N were measured by a Lake Shore 7404 vibrating sample magnetometer (VSM).

The X-ray photoelectron spectroscopy (XPS) measurements were performed on a Thermo ESCALAB 250XI electron spectrometer with a monochromatic Al Kα radiation (hν = 1486.8 eV) and the spot size of all spectra were 650 μm. The DMFDCA was identified qualitatively by a Thermo-Fisher Trace 1300 & ISQ LT GC–MS instrument equipped with a TR-5MS column (15.0 m × 250 μm × 0.25 μm) and quantified by the Agilent 7890A GC equipped with a DB-WAXetr column (30.0 m × 0.25 mm × 0.25 μm) and a flame ionization detector (FID) that was operated at 270 °C.

2.4. Computational method

The binding energies of O_2 were performed by using the Vienna Ab-initio Simulation Package [31,32] (VASP), employing the density functional theory (DFT) and the Projected Augmented Wave [33] (PAW) method. The Perdew-Burke-Ernzerhof (PBE) functional

was used to describe the exchange and correlation effect [34]. In all the cases, the cut-off energy was set to be 450 eV. The Monkhorst-Pack grids [35] were set to be 3 × 3 × 1 for the all the surface calculations. At least 16 Å vacuum layer was applied in z-direction of the slab models, preventing the vertical interactions between slabs. Spin-polarization was contained in all the cases. The Co@NC model was constructed as one mono-layer N doped graphene staying on the top of the (111) surface of Co.

The adsorption energy of O_2 was defined as

$$\Delta E_B = E_{ads} - E_{slab} - E_{O2}$$

where Eads is the electronic energy of the slab with an adsorbed O_2, Eslab is the electronic energy of the clean slab, and E_{O2} is the electronic energy of gaseous oxygen molecule. Under this definition, a more negative value indicates a stronger binding system.

2.5. Catalytic oxidation esterification of HMF

In a typical run, HMF (5.0 mmol), catalyst (100 mg), Na_2CO_3 (30% mol relative to HMF), and methanol (5 mL) were added in a stainless steel reactor equipped with a magnetic stirrer. The reaction mixture was stirred at 100 °C and at 2 MPa O_2. After completion of the reaction, the catalyst was separated and a sample of the liquid mixture was subjected to GC analysis. The conversion of 5-HMF and the yield of products were calculated according to the following equations:

$$\text{HMF conversion} = \left(1 - \frac{\text{Moles of HMF}}{\text{Moles of HMF loaded}}\right) \times 100\%$$

$$\text{Product yield} = \left(1 - \frac{\text{Moles of product}}{\text{Moles of HMF converted}}\right) \times 100\%$$

3. Results and discussion

3.1. Catalyst preparation and characterization

The two-step synthesis of Co@C-N is shown in Fig. 1a. ZIF-67 was firstly synthesized by the modified room-temperature precipitation method [36]. The powder X-ray diffraction (XRD) patterns of synthetic ZIF-67 (Fig. 1b) matched well with a simulated analogue, confirming the formation of pure ZIF-67 crystals. As shown in the SEM image (Fig. 3a), synthetic ZIF-67 was composed of microcrystals with a typical rhombic dodecahedral shape, uniform morphology and high crystallinity.

The Co@C-N materials were formed by a simple thermal decomposition of ZIF-67 under an argon atmosphere and metal ions were reduced *in situ*. Thermogravimetric (TG) analysis indicated that the organic ligands in ZIF-67 began to decompose at ca. 500 °C (Fig. 1c). Therefore, the final set of pyrolyzed temperatures chosen were 600, 700, 800 and 900 °C, resulting in Co@C-N(T), where T represents the thermolysis temperature. The corresponding mass loss is about 28.3–46.6 wt%, which is significantly lower than the theoretical values in the transformation from ZIF-67 to metallic Co (73.3%), implying that carbon-containing materials are generated during the pyrolysis process.

XRD patterns of the Co@C-N materials were shown in Fig. 2a, the peak at about 26.3° corresponds to a typical (0 0 2) interlayer of graphite-type carbon sheets, and other peaks at about 44.2°, 51.5°, and 75.8° are attributed to metallic Co (PDF#. 15-0806). The enhanced peak intensities of the Co diffraction peaks for the Co@C-N(T) at higher calcination temperatures suggests the formation of a Co phase with a higher crystallization degree. The Raman spectra of the samples also revealed characteristic carbon G and D bands, corresponding to the graphitic sp^2-carbon and disoriented carbon, respectively (Fig. 2b) [37]. The I_G/I_D band intensity ratios of Co@C-N(600), Co@C-N(700), Co@C-N(800) and Co@C-N(900) materials are 0.86, 0.97, 1.29 and 1.97, respectively, revealing that the crystallization degree of graphitic carbon becomes better with temperature, which was consistent with the XRD observations.

SEM images indicated that the pyrolyzed nanoparticles roughly retained the polyhedral shape of parent ZIF-67, and shrunk slightly (Fig. 3b). As shown in Fig. 3(d) and Figure S1, the presence of Co nanoparticles encapsulated by a few layered carbon shells and the particle size of Co nanoparticles increased with the pyrolysis temperature. Furthermore, the highly dispersed Co nanoparticles of materials were also observed, which was mainly due to the ordered organic ligands of ZIF-67. Fig. 3(e, f) revealed that the carbon matrices and Co nanoparticles of Co@C-N(800) were crystalline and the lattice fringes with an inter-planar distance of 0.334 nm and 0.204 nm correspond to the C(002) plane and Co (111) [38]. The diffraction rings in the SAED image (Fig. 3c) can be attributed to Co, in good agreement with XRD results.

3.2. Catalyst activity and stability

The selective oxidative esterification of HMF to DMFDCA was performed in the presence of sodium carbonate using methanol as the solvent at 100 °C under 2 MPa oxygen. The results of exploratory catalytic experiments with the different catalytic materials were summarized in Table 1. The parent ZIF-67 showed no activity (entry 1). Pleasingly, the ZIF-67 pyrolysed materials were effective and the yields of DMFDCA were disproportionately affected by the pyrolysis temperature of the ZIF-67 precursors (entries 2–5). Among the four Co@C-N(T) samples, Co@C-N(800) was the most active for the HMF conversion, affording DMFDCA in 99% conversion and 91% yield (entry 4).

With the optimum Co@C-N(800) catalyst in hand, the reaction conditions for the conversion of HMF into DMFDCA were subsequently investigated. It was found that the reaction temperature of 100 °C and oxygen pressure of 2 MPa was optimum in terms of both HMF conversion and DMFDCA yield (Table 1. entries 6–11).

Next, the effect of different strength bases on the Co@C-N(800)-catalyzed oxidation of HMF to DMFDCA in methanol was investigated (Fig. 4a). The introduction of weak bases (i.e., $NaHCO_3$, $KHCO_3$) resulted in a slight increase in DMFDCA yield, while a significant increase in yield from 83% to 91% was obtained when using Na_2CO_3 and K_2CO_3. However, stronger bases (i.e., NaOH, KOH, NaOMe and NaOEt) led to a high HMF conversion but a decrease in DMFDCA yield, indicating that some undesired byproducts were formed. The Co@C-N(800) material can efficiently catalyze the oxidative esterification of HMF, even in the absence of base, to afford DMFDCA in 83% yield (Figure 4 and S2), which can be attributed to the strong basic sites of Co@C-N(800) as evidenced with CO_2-TPD (Figure S3). The DMFDCA yield firstly increased and then decreased with the increasing base concentration, and the optimized content of Na_2CO_3 was 30 mol% with respect to HMF (Figure S4). As shown in Fig. 4b, the yield of DMFDCA reached 83% in only one hour, and such high efficiency have not been reported to date. A 95% yield of DMFDCA was obtained after a prolonged reaction time (12 h). These high conversion and selectivity achieved by Co@C-N can compare well with those reported noble metal based catalysts [4,6–13], even in a lower O_2 pressure (Table 1, entry 7). Furthermore, the non-noble metal catalysts are cost-effective and feasible, especially for large-scale production.

The recyclability of the catalyst was also investigated. After the reaction, the catalyst was dispersed in ethanol solution and was easily separated with an external magnet given the magnetic properties of Co-based material (Fig. 4c). ICP-OES analysis of the reaction solution conformed that the content of Co was below the detection limit, suggesting no obvious Co leaching during the

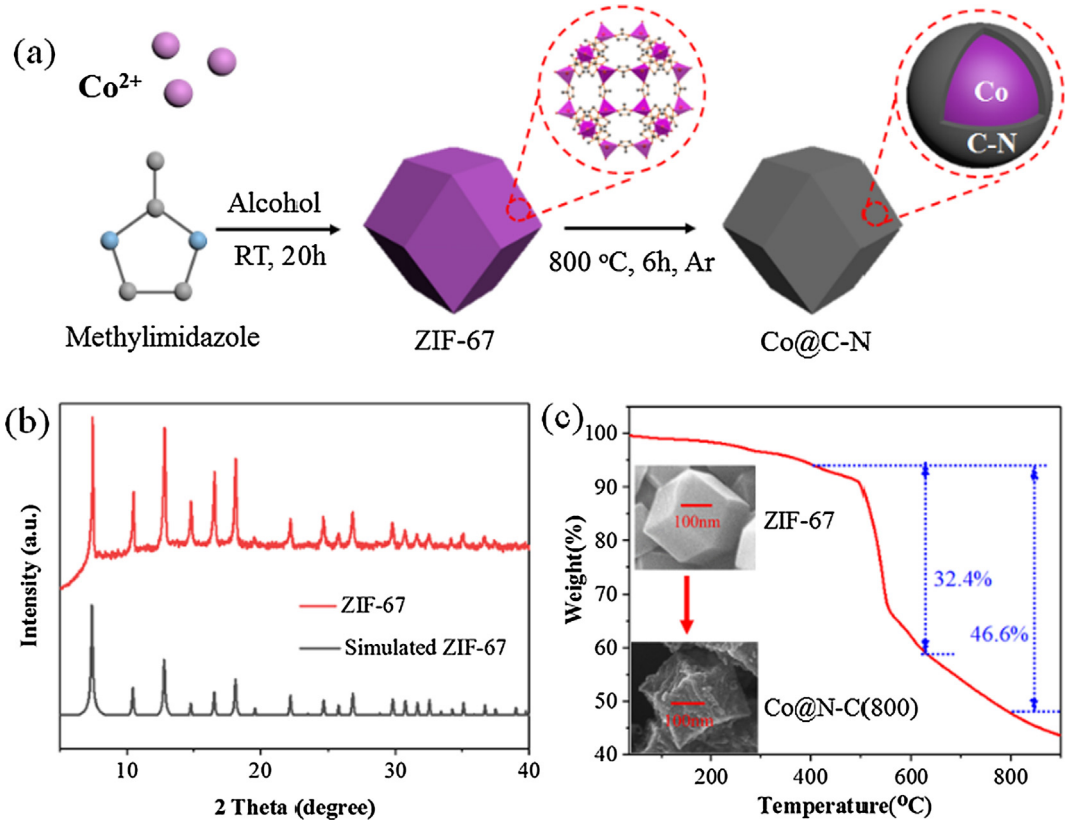

Fig. 1. (a) Synthetic scheme for the preparation of Co@C-N, (b) XRD pattern of ZIF-67, (c) TG curve of ZIF-67 in N_2.

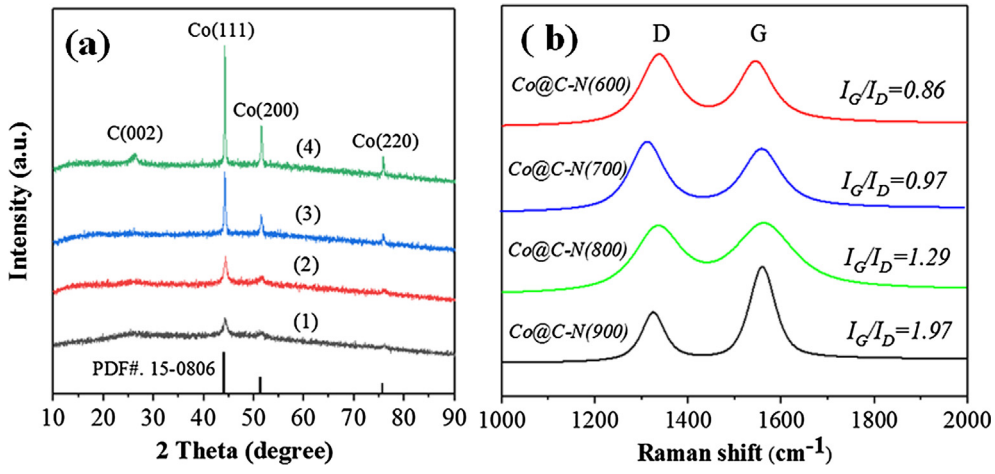

Fig. 2. (a) XRD patterns of (1) Co@C-N(600), (2) Co@C-N(700), (3) Co@C-N(800), and (4) Co@C-N(900); (b) Raman spectra of Co@C-N.

reaction. The isolated catalyst was washed several times with ethanol and subsequently reused in HMF conversion to DMFDCA under identical reaction conditions. These results showed that the activity of the reused catalyst was significantly decreased. Fortunately, after being reduced with H_2 at 400 °C for 1 h, the catalyst could be reused for up to five runs without any apparent loss in efficiency (Fig. 4d). The XRD patterns indicated that the Co diffraction intensity of the reused catalyst (without reduction in H_2) became much weaker (Fig S5), suggesting a partial oxidation of metallic Co occured during the oxidation reaction. After reduction in H_2 at 400 °C for 1 h, the XRD profile was similar to the freshly prepared catalyst (Figure S5), which led to high reactivity of the regenerated Co@C-N(800) material.

3.3. Mechanism study on catalyst activity

To verify the nature of the active sites in Co@C-N(T), a series of Co or carbon-based samples were prepared for the aerobic oxidative esterification of HMF under identical conditions (Table 2). In the absence of any catalyst, HMF conversion was 17% and DMFDCA yield was less than 1% (entry 1). A similar result was obtained when using activated carbon as catalyst, demonstrating that there was no obvious catalytic activity with activated carbon or without the catalyst (entry 2). Note that the C-N composite, synthesized by dipping Co@C-N(800) into aqua regia for 48 h to remove Co (Figure S5), exhibited some activity in the conversion of HMF to DMFDCA (entry 3). Subsequently, the Co@C-N(800) was treated

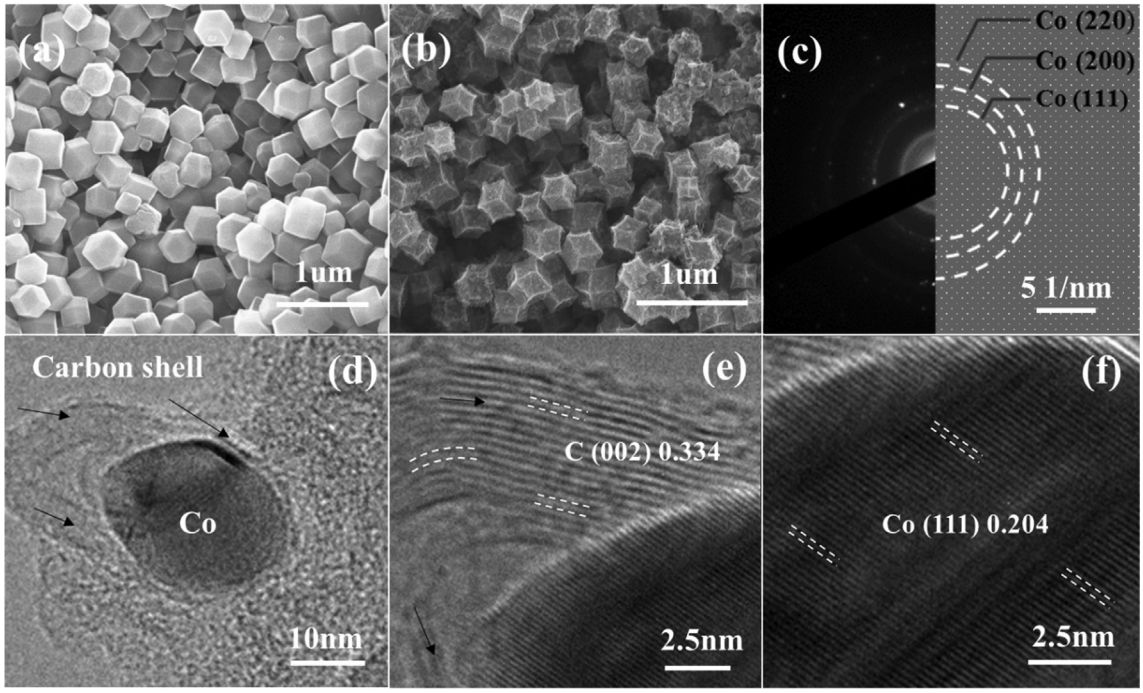

Fig. 3. (a) SEM image of ZIF-67, (b) SEM images of Co@C-N(800), (c) SAED pattern of Co@C-N(800), and (d-f) HRTEM images of Co@C-N(800). Arrows in d and e indicate the direction of the graphitic layers.

Table 1
Conversion of HMF to DMFDCA by Co@C-N.[a]

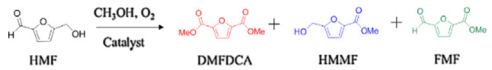

Entry	Catalyst	Temperature(°C)	O_2 (MPa)	Con.(%)	Sel.[b] (%)	Yield (%)		
						DMFDCA	HMMF	FMF
1	ZIF-67	100	2					
2	Co@C-N(600)	100	2	92	93	70	13	3
3	Co@C-N(700)	100	2	96	86	82	7	1
4	Co@C-N(800)	100	2	99	98	91	5	1
5	Co@C-N(900)	100	2	88	90	52	23	4
6[c]	Co@C-N(800)	100	0 (air)	54	<4	<1	<1	2
7[d]	Co@C-N(800)	100	0.1	91	98	77	11	1
8	Co@C-N(800)	100	1	97	98	85	8	2
9	Co@C-N(800)	100	3	99	97	88	6	2
10	Co@C-N(800)	80	2	88	94	60	19	4
11	Co@C-N(800)	120	2	75	89	45	13	9

[a] Condition: HMF (0.5 mmol), Catalyst (100 mg), Na_2CO_3 (30 mol% relative to HMF), methanol (5 mL), 5 h.
[b] Sel. = Yield(DMFDCA + HMMF + FMF)/Con.
[c] 42% of DFF was detected as by-product.
[d] 12h.

at 400 °C in air for 1 h and then reduced under H_2 for another hour to obtain metallic Co (Figure S6), resulting in a negligible DMFDCA yield (entry 4). The physical mixture of metallic Co and activated carbon also showed poor activity (entry 5). Interestingly, a significantly enhanced yield was obtained when mixed with C-N composite (entry 6), suggesting an absolutely essential role of N-doping. For comparison, Co-MOF (Co-BTC) without N was pyrolyzed at 800 °C to generate Co@C(800). However, a relatively low DMFDCA yield of 18% was obtained (entry 7). These control experiments demonstrated the important synergic interactions between Co and C-N composite in the activity of Co@C-N(800) in the oxidative esterification reaction.

To elucidate how the Co nanoparticles work in coordination with N-doping Carbon for the selective oxidation of HMF, the chemical composition and structural features were further characterized. The nitrogen mass contents in Co@C-N(600), Co@C-N(700), Co@C-N(800) and Co@C-N(900) are 9.7, 5.8, 2.1 and 0.6 wt%, respectively (Table S1). Two high-resolution N1s peaks of Co@C-N(T) suggest the presence of two types of nitrogen species, pyridinic N at ~399 eV and graphitic N at ~401 eV (Fig. 5a and e) [19]. The results showed that the relative contents of graphitic N increased with increasing thermolysis temperature, while that of pyridinic N decreased (Fig. 5b), implying a higher graphitization degree at higher temperatures, which are beneficial for high

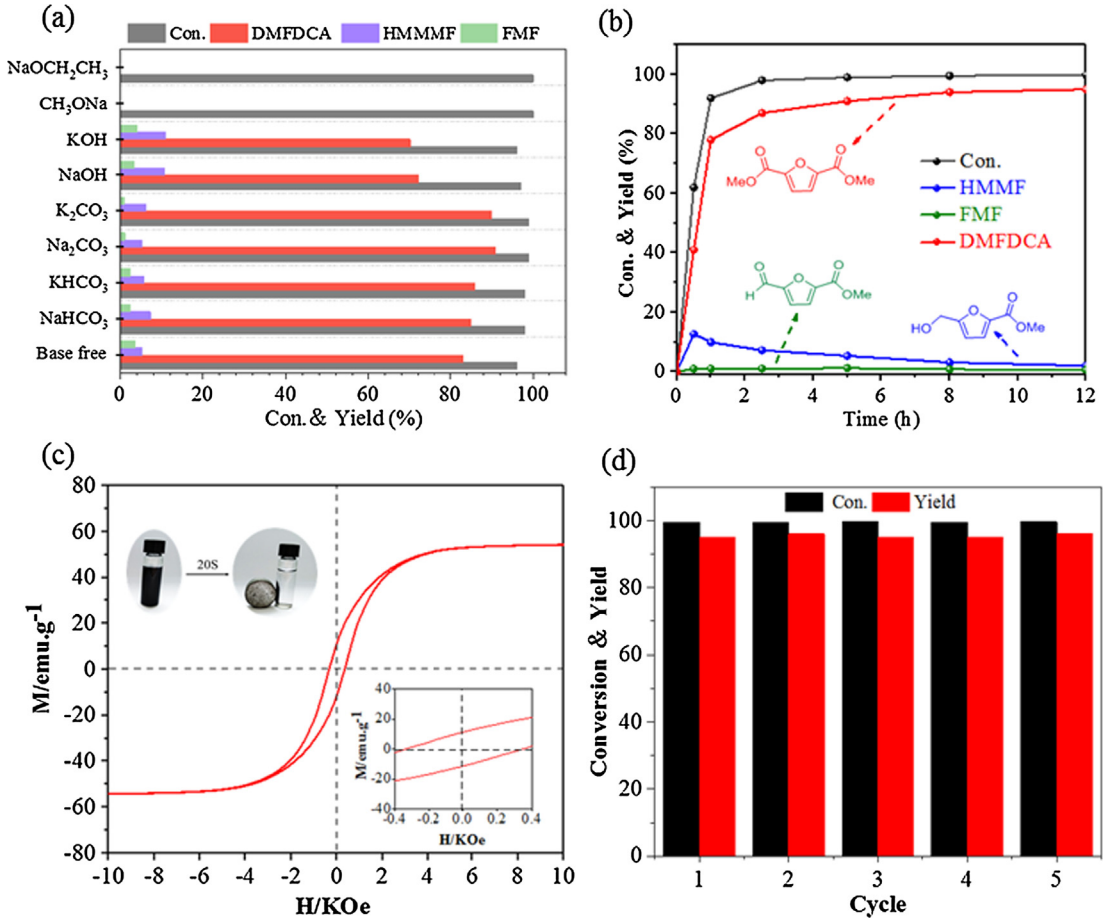

Fig. 4. (a) Conversion of HMF to DMFDCA upon addition of various strength bases. Conditions HMF, (0.5 mmol), catalyst (100 mg), base (30 mol%, relative to HMF), 5 mL methanol, 2 MPa O_2, 100 °C, 5 h; (b) Conversion of HMF to DMFDCA by Co@C-N(800). Conditions: HMF (0.5 mmol), catalyst (100 mg), Na_2CO_3 (30 mol%, relative to HMF), 5 mL methanol, 2 MPa O_2, 100 °C; (c) Magnetic separation of the catalyst after reaction; (d) Reuses of the Co@C-N(800) catalyst for HMF oxidation.

Table 2
The oxidative esterification of HMF in the presence of various catalysts.[a]

Entry	Catalyst	Conversion %	DMFDCA yield %
1	–	21	<1
2	C	25	<1
3	C-N	85	12
4	Co	38	<1
5	Co + C	28	2
6	Co + C-N	86	33
7	Co@C(800)	60	18

[a] Condition: Catalyst (100 mg), HMF (0.5 mmol), Na_2CO_3 (30 mol% relative to HMF), methanol (5 mL), 2 MPa O_2, 100 °C, 5 h.

electronic mobility. The result is in good agreement with the XRD and Raman observations. In addition, the pyridinic N doping produces structural defects in C-N composites to form the O_2 adsorption sites and basic sites. Moreover, the Co nanoparticles encapsulated by carbon shells are believed to affect the properties of outer C-N composites. It has been previous reported that the strong interaction between metal nanoparticles and the graphitic walls can enhance activity of nanocarbon catalysts owing to the electron transfer from metal atoms to carbon shells until their Fermi level reaches equilibrium [39,40]. It is beyond doubt that N-doping facilitates the electronic interaction with nearby carbon/metal atoms to accelerate the formation of the oxygen radical. The Co 2p3/2 spectrum exhibits two prominent bands at ~778.7 eV and ~781.0 eV, readily assigned to Co–Co and Co–C bond respectively (Fig. 5c) [41]. The phenomena that Co–Co bond peak shifts to a higher value than that of Co nanoparticles (778.1) as well as the formation of Co–C bond further prove the electron transfer from metal nanoparticles to C-N composites (Fig. 5f).

Based on the aforementioned analysis, the most active Co@C-N (800) material showed an appropriate nitrogen content and a relatively high ratio of graphitic-N/C, contributing to its balance between the contents and species of nitrogen (Fig. 5d). This balance can result in higher electronic mobility and more active sites [42], which is beneficial for activation and reduction of O_2. The strong electronic interaction between Co atoms and N-doping carbon is prone to generate strong electron acceptors (Co nanoparticles) and electron donors (C-N composites), leading to the high catalytic activity of Co@C-N(800) in the oxidative esterification reaction. As previously reported, both of the electron-poor metal nanoparticles and the electron-rich carbon shells should attract O_2 [43–46] which results in unclear O_2 adsorption sites. Thus, a series of DFT simulations were performed to reveal the O_2 adsorption sites on Co@C-N(800). The Co@NC model was constructed as one mono-layer N doped graphene staying on the top of the (111) surface of Co. As illustrated in Fig. 6a, O2 adsorption on Co sites resulted in the O–O bond cleavage. This indicated that O_2 cannot be adsorbed on Co sites, which also resulted in high adsorption energy of O_2 (3.74 eV). However, the O–O linkage was well maintained since O_2 was adsorbed on C–N sites (Fig. 6b) and the low binding energy (−0.05 eV) further demonstrated that the oxygen molecule was adsorbed and activated on the C–N materials.

It can also be assumed from the simulation results that the –CHO and –OH group of HMF are activated at C–N sites because

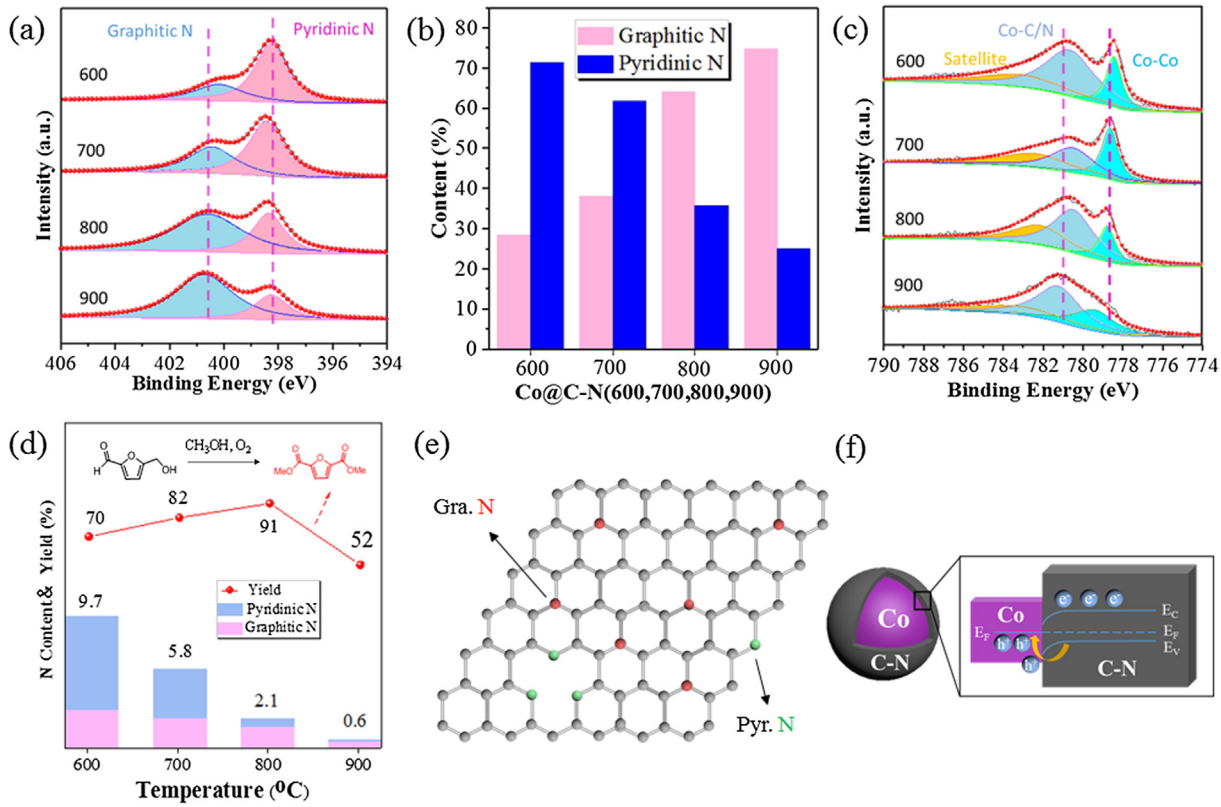

Fig. 5. (a) High-resolution N 1s XPS spectra of Co@C-N (600–900). (b) The relative contents of N species of Co@C-N (600–900). (c) High-resolution Co $2p_{3/2}$ XPS spectra of Co@C-N (600–900). (d) N content and the corresponding DMFDCA yield for Co@C-N (600–900), (e) Possible bonding configurations of N-doped carbon sheels of Co@C-N(800). (f) Schematic illustration of electron transfer between Co nanoparticles and N-doped carbon materials.

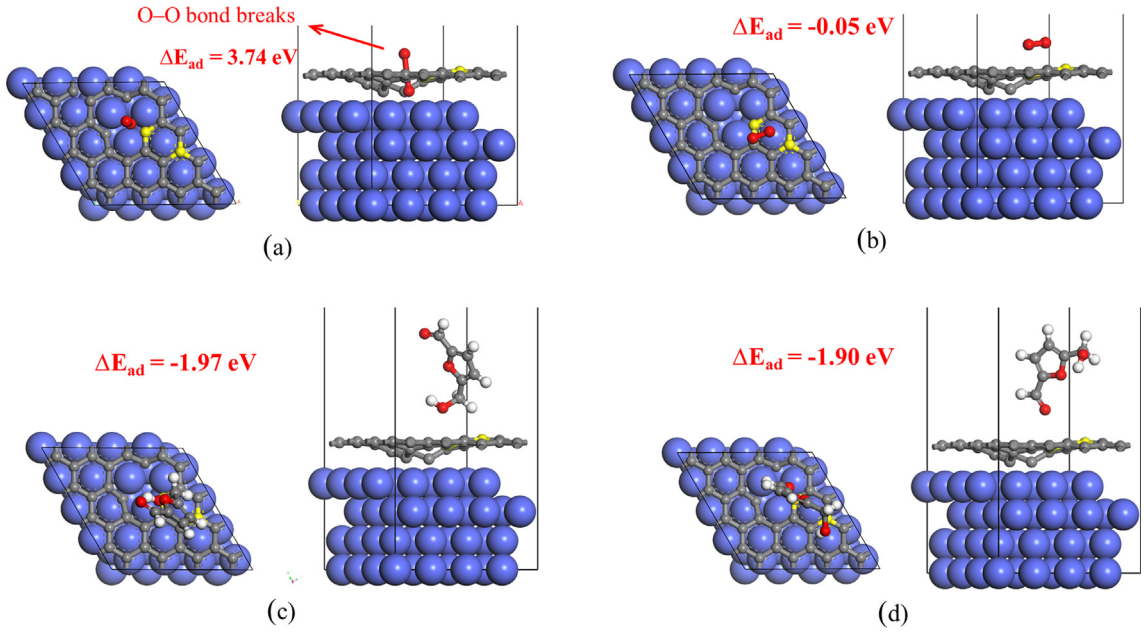

Fig. 6. Schematic model of (a) O_2 adsorption on Co sites, (b) O_2 adsorption on N-doped carbon sites, (c)–OH (HMF) adsorption on C-N sites and (d) –CHO (HMF) adsorption on C-N siteThe brown, gray, blue, and red balls represent C, N, Co and O atoms, respectively.

the size of HMF molecular is larger than O_2 molecualr. As shown in Fig. 6(c, d), the low adsorption energies supported the hypothesis that HMF is activated at C–N sites. On the basis of the conversion-time profiles (Fig. 4b, S2), almost no DFF was detected (Figure S7a). The factor of selective and preferential adsorption for alcohol or aldehyde group in HMF should be excluded as the closely calculated adsorption energy between the –CHO (–1.9 eV) and –OH (–1.97 eV) group. Note that hemiacetal reactions of the aldehyde group can be easily proceeded in alcoholic solvents. Thus, this result was attributed to

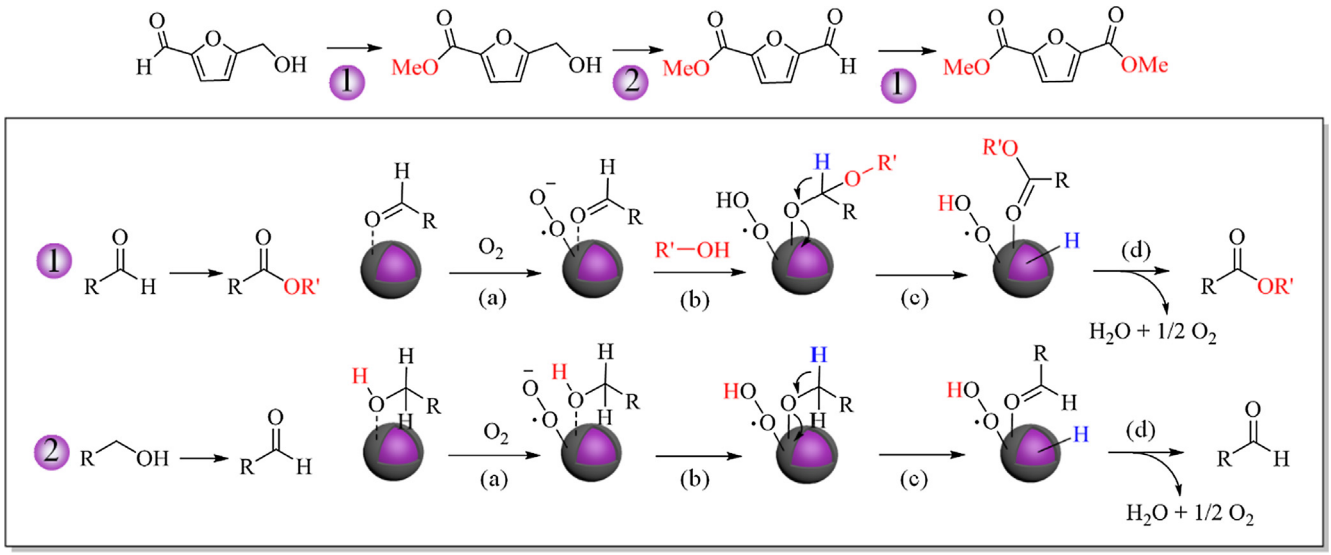

Fig. 7. Plausible mechanism for the conversion HMF to DMFDCA by Co@C-N. (a) Adsorption of O_2 and formation of superoxide anion radical; (b) Superoxide anion radical reacts with alcohol; (c) β-hydride elimination; (d) Oxidation of metal–hydride.

the fact that the oxidative esterification of aldehyde was preferentially occurred than the oxidation of hydroxyl groups of HMF (Figure S7b).

When di-tert-butyl-4-methylphenol (BHT, a free-radical scavenger) was introduced, the yield of DMFDCA decreased (Figure S8a), suggesting that oxygen radical(s) were formed after O_2 adsorption onto the C-N sites. The oxygen radical(s) was(were) further checked by Electron Paramagnetic Resonance (EPR) as shown in Figure S8b. These peaks were typical EPR signals of DMPO-•O^2H adducts, demonstrating the of superoxide anion radical (•O^{2-}) was formed in our catalytic system. It's worth noted that superoxide anion radical was also produced when using Co_xO_y@C-N as catalyst alone [12], but mixing with Ru/C, K-OMS-2 or α-MnO_2 were required to achieve high conversion [12,17,18], indicating an superior role Co@C-N in the oxidative esterification reaction.

On the basis of the reaction process and above analysis, a possible reaction mechanism for the oxidation of HMF to DMFDCA is presented in Fig. 7. First, oxygen molecules are adsorbed and activated at the electron-rich carbon sites adjacent to the pyridinic N (where more structural defects exist), accepting electrons to produce superoxide anion radical. At the same time, aldehyde/alcohol (HMF) can be attracted on C-N sites. Then, the superoxide anion radical reacts with alcohol (MeOH/HMF), producing the corresponding ester/aldehyde by a β-hydride elimination (oxidation of aldehyde to ester via a hemiacetal coordinated intermediate). It is well established that the β-hydride elimination is commonly associated with the formation of H-metal species on the catalyst surface [47–49], so the introduction of an appropriate base can facilitate deprotonation of the H-metal species to regenerate the active catalyst surface.

4. Conclusions

In summary, starting with Co-MOF (ZIF-67) particles as the single template, we prepared Co@C-N materials that are cost effective, effective, stable and reusable catalysts for the oxidative esterification of HMF to DMFDCA. The synthetic Co@C-N composites exhibited excellent activity and selectivity for the DMFDCA production, a result of the nitrogen doping and the electron transfer between Co and C-N composite. Among the four Co@C-N samples synthesized at different temperatures, Co@C-N(800) showed the highest reactivity, which can be attributed to the balance of the contents and species of nitrogen. DFT simulations concluded that oxygen molecular and HMF were adsorbed and activated on C-N sheels. No DFF was observed indicating that the oxidative esterification of aldehyde was preferentially proceed than the oxidation of hydroxyl group of HMF. Most importantly, the detail studied Co@C-N catalyzed oxidative esterification mechanism could promote a devolpement of oxidative esterification reaction, especially for bio-based polymers sector.

Declaration of Competing Interest

The authors declare that they have no known competing financial interests or personal relationships that could have appeared to influence the work reported in this paper.

Acknowledgements

This work was supported by the National Natural Science Foundation of China (No. 21978248), the Natural Science Foundation of Fujian Province of China (No. 2019J06005), and the Energy Development Foundation of the College of Energy, Xiamen University (No. 2017NYFZ02). We also thank the New Zealand Ministry of Business, Innovation and Employment (MBIE) for support through the Catalyst Fund (16-UOA-049-CSG).

Appendix A. Supplementary material

Supplementary data to this article can be found online at https://doi.org/10.1016/j.jcat.2019.11.029.

References

[1] T.A. Werpy, J.E. Holladay, J.F. White, Synthetic Fuels, 2004.
[2] J. Zhu, J. Cai, W. Xie, P.H. Chen, M. Gazzano, M. Scandola, R.A. Gross, Macromolecules 46 (2013) 796–804.
[3] A.J.J.E. Eerhart, A.P.C. Faaij, M.K. Patel, Energy Environ. Sci. 5 (2012) 6407–6422.
[4] E. Taarning, I.S. Nielsen, K. Egeblad, R. Madsen, C.H. Christensen, ChemSusChem 1 (2008) 75–78.
[5] G.Z. Papageorgiou, D.G. Papageorgiou, Z. Terzopoulou, D.N. Bikiaris, Eur. Polym. J. 83 (2016) 202–229.
[6] F. Menegazzo, M. Signoretto, D. Marchese, F. Pinna, M. Manzoli, J. Catal. 326 (2015) 1–8.

[7] F. Li, X.-L. Li, C. Li, J. Shi, Y. Fu, Green Chem. 20 (2018) 3050–3058.
[8] J. Du, H. Fang, H. Qu, J. Zhang, X. Duan, Y. Yuan, Appl. Catal. A 567 (2018) 80–89.
[9] O. Casanova, S. Iborra, A. Corma, J. Catal. 265 (2009) 109–116.
[10] A. Cho, S. Byun, J.H. Cho, B.M. Kim, ChemSusShem 12 (2019) 2310–2317.
[11] A. Buonerba, S. Impemba, A.D. Litta, C. Capacchione, S. Milione, A. Grassi, ChemSusChem 11 (2018) 3139–3149.
[12] A. Salazar, P. Hünemörder, J. Rabeah, A. Quade, R.V. Jagadeesh, E. Mejia, ACS. Sustain. Chem. Eng. 7 (2019) 12061–12068.
[13] D.S. Mannel, J. King, Y. Preger, M.S. Ahmed, T.W. Root, S.S. Stahl, ACS Catal. 8 (2018) 1038–1047.
[14] R.V. Jagadeesh, H. Junge, M.-M. Pohl, J.r. Radnik, A. Brückner, M. Beller, J. Am. Chem. Soc. 2013, 135, 10776–10782.
[15] C. Bai, A. Li, X. Yao, H. Liu, Y. Li, Green Chem. 18 (2016) 1061–1069.
[16] K.-K. Sun, S.-J. Chen, Z.-L. Li, G.-P. Lu, C. Cai, Green Chem. 21 (2019) 1602–1608.
[17] J. Deng, H.J. Song, M.S. Cui, Y.P. Du, Y. Fu, ChemSusChem 7 (2014) 3334–3340.
[18] Y. Sun, H. Ma, X. Jia, J. Ma, Y. Luo, J. Gao, J. Xu, ChemCatChem 8 (2016) 2907–2911.
[19] W. Zhong, H. Liu, C. Bai, S. Liao, Y. Li, ACS Catal. 5 (2015) 1850–1856.
[20] Q. Zhu, F. Wang, F. Zhang, Z. Dong, Nanoscale 11 (2019) 17736–17745.
[21] H. Zhou, S. Hong, H. Zhang, Y. Chen, H. Xu, X. Wang, Z. Jiang, S. Chen, Y. Liu, Appl. Catal., B (2019) 117767.
[22] K. Shen, X. Chen, J. Chen, Y. Li, ACS Catal. 6 (2016) 5887–5903.
[23] K. Murugesan, T. Senthamarai, M. Sohail, A.S. Alshammari, M.M. Pohl, M. Beller, R.V. Jagadeesh, Chem. Sci. 9 (2018) 8553–8560.
[24] R.V. Jagadeesh, K. Murugesan, A.S. Alshammari, H. Neumann, M.-M. Pohl, J. Radnik, M. Beller, Science 358 (2017) 326–332.
[25] X. Ma, Y.X. Zhou, H. Liu, Y. Li, H.L. Jiang, Chem. Commun. 52 (2016) 7719–7722.
[26] A.J. Howarth, Y. Liu, P. Li, Z. Li, T.C. Wang, J.T. Hupp, O.K. Farha, Nat. Rev. Mater. 1 (2016) 15018.
[27] J.K. Sun, Q. Xu, Energy Environ. Sci. 7 (2014) 2071–2100.
[28] O.M. Yaghi, M. O'Keeffe, N.W. Ockwig, H.K. Chae, M. Eddaoudi, J. Kim, Nature 423 (2003) 705.
[29] B. Liu, H. Shioyama, T. Akita, Q. Xu, J. Am. Chem. Soc. 130 (2008) 5390–5391.
[30] Y. Feng, G. Yan, T. Wang, W. Jia, X. Zeng, J. Sperry, Y. Sun, X. Tang, T. Lei, L. Lin, Green Chem. 21 (2019) 4319–4323.
[31] G. Kresse, J. Furthmüller, Phys. Rev. B 54 (1996) 11169–11186.
[32] G. Kresse, J. Hafner, Phys. Rev. B 49 (1994) 14251–14269.
[33] P.E. Blöchl, Phys. Rev. B 50 (1994) 17953–17979.
[34] J.P. Perdew, K. Burke, M. Ernzerhof, Phys. Rev. Lett. 77 (1996) 3865–3868.
[35] H.J. Monkhorst, J.D. Pack, Phys. Rev. B 13 (1976) 5188.
[36] Y. Lu, Y. Wang, H. Li, Y. Lin, Z. Jiang, Z. Xie, Q. Kuang, L. Zheng, A.C.S. Appl, Mater. Interfaces 7 (2015) 13604–13611.
[37] M. Zhang, Q. Dai, H. Zheng, M. Chen, L. Dai, Adv. Mater. (2018) 30.
[38] W. Feng, Y. Wang, J. Chen, B. Li, L. Guo, J. Ouyang, D. Jia, Y. Zhou, J. Mater. Chem. C 6 (2018) 10–18.
[39] D. Deng, L. Yu, X. Chen, G. Wang, L. Jin, X. Pan, J. Deng, G. Sun, X. Bao, Angew. Chem. Int. Ed. 52 (2013) 371–375.
[40] G. Wu, K.L. More, C.M. Johnston, P. Zelenay, Science 332 (2011) 443–447.
[41] J. Meng, C. Niu, L. Xu, J. Li, X. Liu, X. Wang, Y. Wu, X. Xu, W. Chen, Q. Li, Z. Zhu, D. Zhao, L. Mai, J. Am. Chem. Soc. 139 (2017) 8212–8221.
[42] C. Hu, L. Dai, Angew. Chem. Int. Ed. 55 (2016) 11736–11758.
[43] L. Zhang, A. Wang, W. Wang, Y. Huang, X. Liu, S. Miao, J. Liu, T. Zhang, ACS Catal. 5 (2015) 6563–6572.
[44] H. Watanabe, S. Asano, S.-I. Fujita, H. Yoshida, M. Arai, ACS Catal. 5 (2015) 2886–2894.
[45] H. Chen, K. Shen, Q. Mao, J. Chen, Y. Li, ACS Catal. 8 (2018) 1417–1426.
[46] H. Su, K.X. Zhang, B. Zhang, H.H. Wang, Q.Y. Yu, X.H. Li, M. Antonietti, J.S. Chen, J. Am. Chem. Soc. 139 (2017) 811–818.
[47] M. Huang, Y. Li, Y. Li, J. Liu, S. Shu, Y. Liu, Z. Ke, Chem. Commun. 55 (2019) 6213–6216.
[48] S. Sarina, S. Bai, Y. Huang, C. Chen, J. Jia, E. Jaatinen, G.A. Ayoko, Z. Bao, H. Zhu, Green Chem. 16 (2014) 331–341.
[49] S.E. Davis, M.S. Ide, R.J. Davis, Green Chem. 15 (2013) 17–45.